

Electronic Supplementary Information

Polydopamine-coated magnetic mesoporous silica nanoparticles for multimodal cancer theranostics†

Menghan Shi^{a,b}, Jiulong Zhang^c, Jingchao Li^b, Yu Fan^b, Jianhong Wang^b, Wenjie Sun^b, Hong Yang^{a,*}, Chen Peng^{c,*}, Mingwu Shen^b, Xiangyang Shi^{b,*}

^aThe Key Laboratory of Resource Chemistry of Ministry of Education, Shanghai Key Laboratory of Rare Earth Functional Materials, and Shanghai Municipal Education Committee Key Laboratory of Molecular Imaging Probes and Sensors, Shanghai Normal University, Shanghai 200234, People's Republic of China

^bCollege of Chemistry, Chemical Engineering and Biotechnology, Donghua University, Shanghai 201620, People's Republic of China

^cDepartment of Radiology, Shanghai Tenth People's Hospital, Tongji University, Shanghai 200072, People's Republic of China

* To whom correspondence should be addressed. E-mail addresses: yanghong@shnu.edu.cn (H. Yang), pengchen_1985@163.com (C. Peng) and xshi@dhu.edu.cn (X. Shi)

Experimental section

Materials. Tetraethyl orthosilicate (TEOS), (3-aminopropyl)triethoxysilane (APTES) and dopamine hydrochloride were obtained from Sigma-Aldrich (St. Louis, MO). Octadecyltrimethoxysilane (C₁₈TMS) was purchased from Acros Organics (New Jersey, NJ). 1-(3-Dimethylaminopropyl)-3-ethylcarbodiimide hydrochloride (EDC·HCl) and *N*-hydroxysuccinimide (NHS) were purchased from GL Biochem. (Shanghai, China). Anhydrous sodium carbonate, isopropanol and ammonia solution (25-28%) were purchased from Shanghai Lingfeng Chemical Reagent Co., Ltd. (Shanghai, China). Iron (III) chloride hexahydrate, trisodium citrate dihydrate and anhydrous sodium acetate were purchased from Sinopharm Chemical Reagent Ltd. (Shanghai, China). Dulbecco's modified Eagle's medium (DMEM), fetal bovine serum (FBS), penicillin, streptomycin, and pancreatin were obtained from Gibco (Grand Island, NY). A Milli-Q Plus 185 water purification system (Millipore, Bedford, MA) was used to treat water to have a resistivity higher than 18.2 MΩ.cm. All reagents were used as received without further purification. 4T1 cancer cells (a mouse mammary carcinoma cell line) were from Institute of Biochemistry and Cell Biology (the Chinese Academy of Sciences, Shanghai, China).

Synthesis of HMS-Fe₃O₄ NPs. Citrate-stabilized USIONPs with a mean size of 2.3 nm were prepared according to our previous work.¹ HMS NPs were synthesized according to the literature.² To modify HMS NPs with primary amines, we followed the protocol according to the literature.³ In brief, HMS NPs (100 mg) were dispersed in alcohol (100 mL) and 1 mL of APTES was dropwise added into the above solution under vigorous magnetic stirring at room temperature for 12 h. The product was washed with water for several times by centrifugation/redispersion and lyophilized to obtain the aminated HMS NPs (for short, HMS-NH₂). Then the formed HMS-NH₂ NPs were used to load USIONPs through an EDC-mediated coupling chemistry. In a typical synthesis, the carboxyl

groups of citrate-stabilized USIONPs (50 mL, 58 mg) were activated by EDC (2 mL, 134 mg) and NHS (1 mL, 87 mg) for 3 h. Then an aqueous solution of HMS-NH₂ NPs (1 mL, 174 mg) was added into the above solution of activated USIONPs. The mixture was continuously stirred at room temperature for 3 days. Afterwards, the product was washed with water by centrifugation (6,000 rpm, 10 min) and redispersion in water for 4 times to yield HMS-Fe₃O₄ NPs. To optimize the loading of USIONPs within HMS NPs, we selected different mass ratios of USIONPs/HMS-NH₂ at 4:1, 3:1, 2:1, and 1:1, respectively.

Synthesis of HMS-Fe₃O₄@PD NPs. To camouflage PD onto the surface of HMS-Fe₃O₄ NPs, HMS-Fe₃O₄ NPs (1 mg/mL) were dispersed in 50 mL of tris buffer solution (10 mM, pH = 8.5) containing dopamine (0.12 mg/mL). After stirring at room temperature for 24 h to allow for the self-polymerization of dopamine, the final particles were centrifuged and washed several times with water to remove the excess free dopamine. The final product (for short, HMS-Fe₃O₄@PD NPs) was resuspended in water for further study.

Characterization techniques. Thermogravimetric analysis (TGA) was performed by a TG 209 F1 thermogravimetric analyzer (NETZSCH Instruments Co., Ltd., Bavaria, Germany) under nitrogen atmosphere in a temperature range of 10-900 °C. Zeta potential and dynamic light scattering (DLS) measurements were conducted using a Malvern Zetasizer Nano ZS model ZEN3600 (Worcestershire, UK) equipped with a standard 633 nm laser. UV-vis spectrometry was carried out using a Lambda 25 UV-vis spectrophotometer (Perkin Elmer, Boston, MA). Transmission electron microscopy (TEM) was used to observe the morphology of samples at an operating voltage of 200 kV (TEM, JEOL 2010F, Tokyo, Japan). A typical TEM sample was prepared by depositing an aqueous sample solution onto carbon-coated copper grid and air-dried before measurements. Fe concentrations were analyzed using a Leeman Prodigy inductively coupled plasma-optical emission

spectroscopy (ICP-OES, Hudson, NH).

MR/PA imaging and photothermal properties of HMS-Fe₃O₄@PD NPs. T₁ relaxometry measurements were performed using an 0.5 T NMI20 Analyst NMR Analyzing and Imaging system (Shanghai NIUMAG Corporation, Shanghai, China). USIONPs and HMS-Fe₃O₄@PD NPs dispersed in water at different Fe concentrations (0.1, 0.3, 0.6, 0.9, 1.2 or 2.4 mM) were filled into each 1-mL Eppendorf tube. The parameters were set as follows: TR = 400 ms, TE = 20 ms, resolution = 156 mm × 156 mm, and section thickness = 0.5 mm. The T₁ relaxation rate was obtained by linearly fitting the inverse T₁ relaxation time (1/T₁) as a function of Fe concentration. For PA imaging, solutions of HMS-Fe₃O₄@PD NPs at different Fe concentrations (5, 10, 20, 50, 100 and 200 µg/mL, respectively) were filled into thin tubes and tested with a Vevo®LAZR photoacoustic (PA) imaging system. The used laser wavelength was 808 nm.

To study the photothermal property of HMS-Fe₃O₄@PD NPs, 0.5 mL of NP solutions at different Fe concentrations (10, 20, 50, 100 or 200 µg/mL) were respectively irradiated by an 808 nm laser at a power intensity of 1.2 W/cm² for 5 min. Next, 0.5 mL of HMS-Fe₃O₄@PD NPs at the Fe concentration of 200 µg/mL or water was laser irradiated at different power intensities (0.2, 0.4, 0.6, 0.8, 1.0 or 1.2 W/cm²) for 5 min, respectively. A thermocouple (Shenzhen Everbest Machinery Industry Co., Ltd., Shenzhen, China) was used to record the temperature changes during laser irradiation. We performed quantitative analysis of the photothermal conversion efficiency (η) of the HMS-Fe₃O₄@PD NPs according to the literature.⁴ In brief, 0.5 mL of HMS-Fe₃O₄@PD NPs at the Fe concentration of 200 µg/mL was placed in a 1-mL Eppendorf tube and irradiated by an 808 nm laser at a power intensity of 1.2 W/cm². The temperature of the HMS-Fe₃O₄@PD NP solution was recorded every 10 s using a thermocouple. The η was calculated by the following equation:

$$\eta = \frac{hS(T_{Max} - T_{Sur}) - Q_S}{I(1 - 10^{-A\lambda})} \quad (1)$$

Where h is the heat transfer coefficient, S the surface area of the sample cuvette, T_{Max} the steady-state temperature, T_{Sur} the temperature of the surroundings, Q_S the heat associated with the light absorbance of the solution, I the incident laser power, and $A\lambda$ the absorbance at a wavelength of 808 nm. In addition, the photothermal stability of HMS-Fe₃O₄@PD NPs was tested by irradiating the sample for 260 s (1.2 W/cm²) and then cooling down. The laser on/off process was performed for 5 times.

Cytotoxicity, hemolysis, and cellular uptake assays. 4T1 cells were selected as a model to assess the *in vitro* cytotoxicity of the HMS-Fe₃O₄@PD NPs. In brief, 1×10⁴ 4T1 cells suspended in 100 μL DMEM were seeded into each well of a 96-well plate and incubated overnight in a 5% CO₂ incubator at 37 °C. Then, the cell culture medium in each well was removed and the HMS-Fe₃O₄@PD NP solutions formulated in DMEM at different Fe concentrations (5, 10, 20, 50, 100 200 and 250 μg/mL) were added to each well. After incubation for 24 h, the cell culture medium was discarded and the cells were washed three times with phosphate buffer saline (PBS). Afterwards, 100 μL of DMEM containing 10 μL of CCK-8 solution was added into each well and the cells were incubated for additional 4 h. Then, the absorbance at 540 nm in each well was measured with a Multiskan MK3 ELISA reader (Thermo Scientific, Waltham, MA). The absorbance of the control group without treatments was used as a reference to calculate the cell viability.

Hemolysis assay was performed according to the literature.⁵ Fresh human blood sample stabilized with ethylenediaminetetraacetic acid (EDTA) was kindly supplied by Shanghai Tenth People's Hospital (Shanghai, China) and used with the permission by the ethical committee of Shanghai Tenth People's Hospital. The blood sample was centrifuged (1,000 rpm, 10 min) to

remove the supernatant and washed with PBS for 5 times to completely remove serum and obtain the human red blood cells (HRBCs). Then, the HRBCs were 10 times diluted with PBS for further use. The diluted HRBC suspension (0.1 mL) was transferred into 1.5 mL Eppendorf tubes prefilled with 0.9 mL water (as positive control), 0.9 mL PBS (as negative control), and 0.9 mL PBS containing USIONPs or HMS-Fe₃O₄@PD NPs at different Fe concentrations (0-200 µg/mL), respectively. The above mixtures were incubated at 37 °C for 2 h, followed by centrifugation (10, 000 rpm, 1 min). The absorbance of the supernatants related to hemoglobin was recorded with a Lambda 25 UV-vis spectrophotometer (Perkin Elmer, Waltham, MA) at 541 nm. The hemolytic percentage (HP) was calculated using the following equation:

$$\text{HP}(\%) = \frac{D_t - D_{nc}}{D_{pc} - D_{nc}} \times 100\% \quad (2)$$

where D_t is the absorbance of the test samples; D_{pc} and D_{nc} are the absorbances of the positive and negative control, respectively.

In vitro cellular uptake of HMS-Fe₃O₄@PD NPs by 4T1 cells was evaluated by quantitative ICP-OES analysis according to the literature.⁴ Briefly, 4T1 cells were seeded into 12-well cell culture plate at a density of 2×10^6 cells/well with 2 mL of regular DMEM. After overnight culture, the medium was replaced with fresh medium containing PBS or HMS-Fe₃O₄@PD NPs at different final Fe concentrations (5-200 µg/mL), and the cells were incubated in 5% CO₂ at 37 °C for an additional 12 h. Subsequently, the cells were washed 3 times with PBS, trypsinized, centrifuged, and resuspended in PBS. The cells were counted and lysed using an aqua regia solution (1.0 mL) to digest both the cells and NPs. Each sample was diluted with 1.0 mL of water before the quantification of Fe concentration with ICP-OES.

***In vitro* photothermal ablation of cancer cells.** 4T1 cells were seeded in 96-well plates at a

density of 1×10^4 cells per well with 100 μL of fresh DMEM and cultured overnight. Then, the medium in each well was replaced with mixture of 90 μL of fresh DMEM and 10 μL of HMS- $\text{Fe}_3\text{O}_4@PD$ NPs (in PBS) at Fe concentrations ranging from 0 to 200 $\mu\text{g}/\text{mL}$. After 4 h culture, the cells were rinsed with PBS for 3 times and then irradiated by an 808 nm laser ($1.2 \text{ W}/\text{cm}^2$) for 5 min. Then the cells were incubated for another 2 h. The cell viability of each group was determined by CCK-8 assay as described above.

To visualize the photothermal ablation of cancer cells *in vitro*, 4T1 cells were seeded into a 24-well plate at the density of 1×10^5 cells per well in 1 mL of DMEM and then cultured overnight. The cells were incubated with PBS (control) or HMS- $\text{Fe}_3\text{O}_4@PD$ NPs at the Fe concentration of 200 $\mu\text{g}/\text{mL}$, respectively for 4 h. After that, the cells were washed with PBS and exposed to an 808 nm laser ($1.2 \text{ W}/\text{cm}^2$) for 5 min. Then, the cells were cultured in DMEM containing calcein-AM (to stain living cells with green fluorescence) and propidium iodide (PI) (to stain dead cells with red fluorescence) according to the standard protocol.⁶ The cells were observed using an Axio Vert. A1 inverted fluorescence microscope (Carl Zeiss, Jena, Germany) with a magnification of $200 \times$ for each sample.

***In vivo* MR/PA/thermal imaging of a xenografted tumor model.** All the animal experiments were performed following the guidelines of ethical committee of Shanghai Tenth people's Hospital and also the policy of the National Ministry of Health. Female 5-week-old BAIB/c nude mice (15-20 g) were purchased from Shanghai Slac Laboratory Animal Center (Shanghai, China). To establish the xenograft tumor model, mice were subcutaneously injected with 4×10^5 4T1 cancer cells/mouse in the right hind leg. When the tumor volume reached $0.5\text{-}1 \text{ cm}^3$ at about 2 weeks postinjection, the tumor-bearing mice were anesthetized by intraperitoneal injection of pentobarbital sodium (40 mg/kg) and then intravenously injected with a PBS solution (0.15 mL) containing USIONPs or

HMS-Fe₃O₄@PD NPs ([Fe] = 200 μg/mL) for MR imaging.

The mouse model of lymph node metastasis was established according to a previous protocol.⁷ Briefly, 1×10^5 4T1 cells suspended in 0.1 mL of PBS were subcutaneously injected into the 4th abdominal mammary fat pad of the BALB/c mice. After 21 days, tumors appeared in the right hind leg lymph node, mainly due to the lymphatic circulation. Then, the tumor-bearing mice were anesthetized and intravenously injected with a PBS solution (0.15 mL) containing USIONPs or HMS-Fe₃O₄@PD NPs ([Fe] = 200 μg/mL) for MR imaging. Then, the mice were euthanized to extract the normal and tumor lymphoid tissues. The collected lymphoid tissues were fixed with 5% paraformaldehyde, embedded in paraffin, and sectioned for Hematoxylin-Eosin (H&E) staining according to a standard protocol.⁸

For *in vivo* PA imaging, HMS-Fe₃O₄@PD NPs were formulated into a PBS solution at the Fe concentration of 200 μg/mL (0.15 mL) and injected into each tumor-bearing nude mouse through the tail vein. Then, the PA images were acquired and PA signal intensity of the tumors were recorded using Vevo®LAZR system with an 808 nm laser at different time points (0, 20, 40, 60, 80 and 100 min, respectively) postinjection.

For *in vivo* thermal imaging, each 4T1 tumor-bearing mouse was intratumorally injected with 0.1 mL PBS or PBS solution of HMS-Fe₃O₄@PD NPs (200 μg/mL). At 30 min postinjection, the tumor of each mouse was irradiated with an 808 nm laser (1.2 W/cm²) for 300 s. The photothermal medical device (FLIR A300, IRS System Inc., Shanghai, China) coupled with an infrared camera was used to record the dynamic whole-body infrared thermal images.

***In vivo* PTT and combinational therapy of tumors.** The 4T1 tumor-bearing mice were randomly divided into 5 groups (n = 5 for each group). In Group 1, each mouse was anesthetized and then intratumorally injected with 0.1 mL of PBS. In Group 2, each mouse was intratumorally

injected with HMS-Fe₃O₄@PD NPs (200 µg/mL, in 0.1 mL PBS). In Group 3, each mouse was treated with radiotherapy (RT). In Group 4, each mouse was intratumorally injected with HMS-Fe₃O₄@PD NPs (200 µg/mL, in 0.1 mL PBS) and the tumors were then exposed to an 808 nm laser (1.2 W/cm²) for 5 min. In Group 5, each mouse was intratumorally injected with HMS-Fe₃O₄@PD NPs (200 µg/mL, in 0.1 mL PBS) and the tumors were then exposed to an 808 nm laser (1.2 W/cm²) for 5 min, followed by a systemic RT. After the different treatments, the weights of mice were recorded with a counter balance and the tumor sizes of mice were measured with a digital vernier caliper. The tumor volume, relative tumor volume and survival rate of the mice in different groups were recorded according to the literature.⁶

Histological examinations. In order to evaluate the therapeutic efficiency, 4T1 tumor-bearing mice in each group were euthanized after 4 h of treatments to extract the tumor tissues. Then the collected tumors were fixed with 5% paraformaldehyde, embedded in paraffin, and sectioned for H&E and TdT-mediated dUTP Nick-End Labeling (TUNEL) staining using standard protocols.⁹ The stained tumor sections were observed under a Leica DM IL LED inverted phase contrast microscope with a magnification of 100 × for each sample. The number of TUNEL-positive cells (apoptotic cells) in each specimen was counted and the percentages of apoptotic cells were calculated from five random fields of the images.

To further evaluate the *in vivo* biosafety of the treatments, the 4T1 tumor-bearing mice in each group were euthanized after 1 day of treatment to extract heart, liver, spleen, lung and kidney. The collected organs were fixed, embedded, sectioned and H&E stained according to standard protocols.⁹ The morphology of the stained organ sections was observed using a Leica DM IL LED inverted phase contrast microscope with a magnification of 100 × for each sample.

***In vivo* biodistribution.** HMS-Fe₃O₄@PD NPs ([Fe] = 200 µg/mL, in 200 µL PBS) were

intravenously injected to each tumor-bearing mouse via the tail vein. The mice were euthanized at 1, 24 and 96 h postinjection and the heart, liver, spleen, lung, kidney, and tumor were extracted and weighed. The organs were then cut into 1-2 mm² pieces and digested by *aqua regia* for 24 h. The mice injected with PBS (200 μL PBS for each mouse) were used as control. Then, the Fe content in these organs and tumor was measured by ICP-OES.

Statistical analysis. One-way analysis of variance (ANOVA) statistical method was performed to evaluate the experimental data. A value of 0.05 was selected as the significance level and the data were indicated with (*) for $p < 0.05$, (**) for $p < 0.01$, and (***) for $p < 0.001$, respectively.

Table S1. Surface potentials of HMS NPs and HMS-NH₂ NPs.

Sample	Surface potential (mv)
HMS NPs	-24.4 ± 0.98
HMS-NH ₂ NPs	6.9 ± 0.21

Table S2. The r₁ relaxivity of HMS-Fe₃O₄ NPs prepared with different HMS-NH₂/Fe₃O₄ mass ratios.

HMS-NH ₂ /Fe ₃ O ₄ feeding mass ratio	HMS-NH ₂ /Fe ₃ O ₄ mass ratio	r ₁ relaxivity (mM ⁻¹ s ⁻¹)
1:1	1:0.54	0.678
1:2	1:0.68	0.897
1:3	1:0.83	1.273
1:4	1:0.89	n/a

Table S3. Hydrodynamic size, surface potential, and PDI of HMS NPs, HMS-Fe₃O₄ NPs, and HMS-Fe₃O₄@PD NPs.

Sample	Hydrodynamic size (nm)	Surface potential (mV)	PDI
HMS NPs	256.9 ± 0.89	-24.43 ± 0.98	0.24 ± 0.01
HMS-Fe ₃ O ₄ NPs	310.5 ± 1.13	-7.16 ± 0.76	0.56 ± 0.03
HMS-Fe ₃ O ₄ @PD NPs	417.8 ± 0.84	-14.31 ± 0.68	0.18 ± 0.02

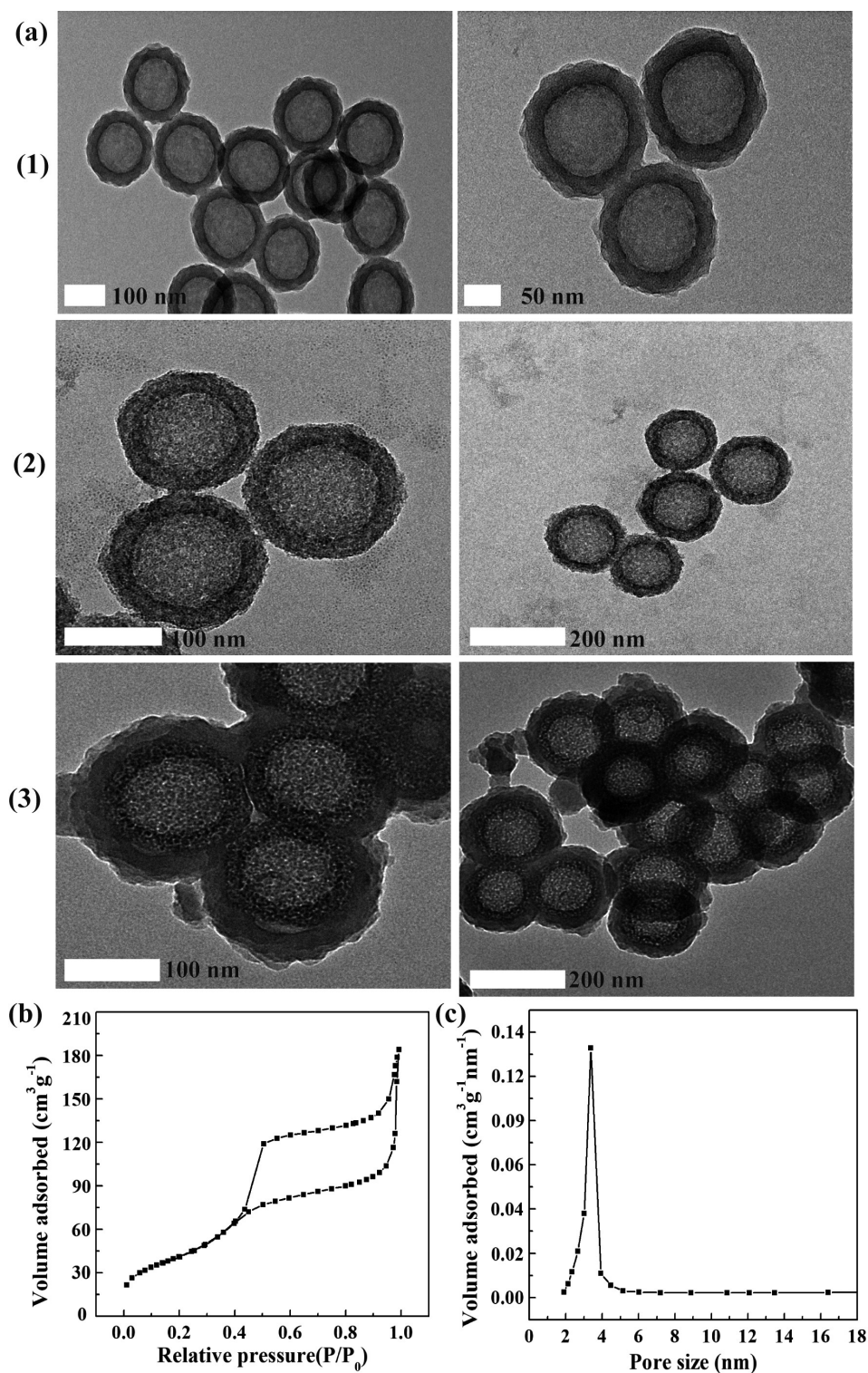


Fig. S1. (a) High-resolution TEM images of HMS-NH₂ NPs (1), HMS-Fe₃O₄ NPs (2) and HMS-Fe₃O₄@PD NPs (3). N₂ adsorption/desorption isotherms (b) and corresponding pore size distribution curve (c) of HMS-NH₂. The surface area and average pore diameter of the particles were determined to be 283.98 m²/g and 3.5 nm, respectively

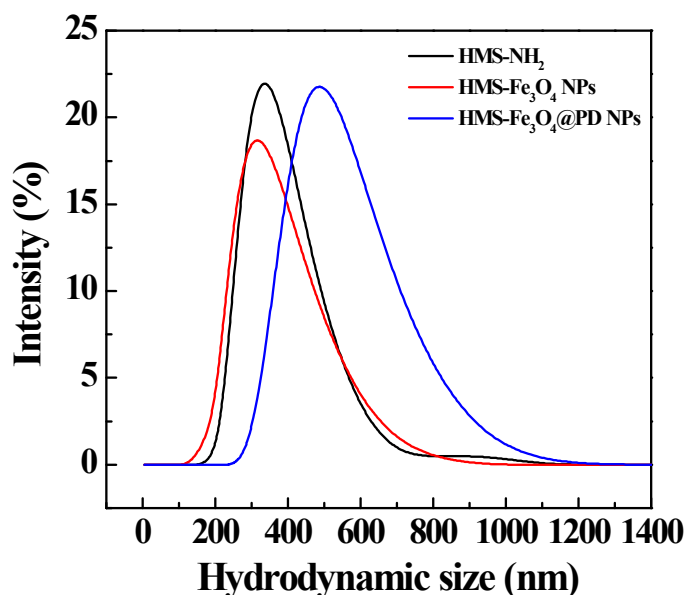


Fig. S2. Hydrodynamic size distribution of HMS-NH₂, HMS-Fe₃O₄ NPs, and HMS-Fe₃O₄@PD NPs.

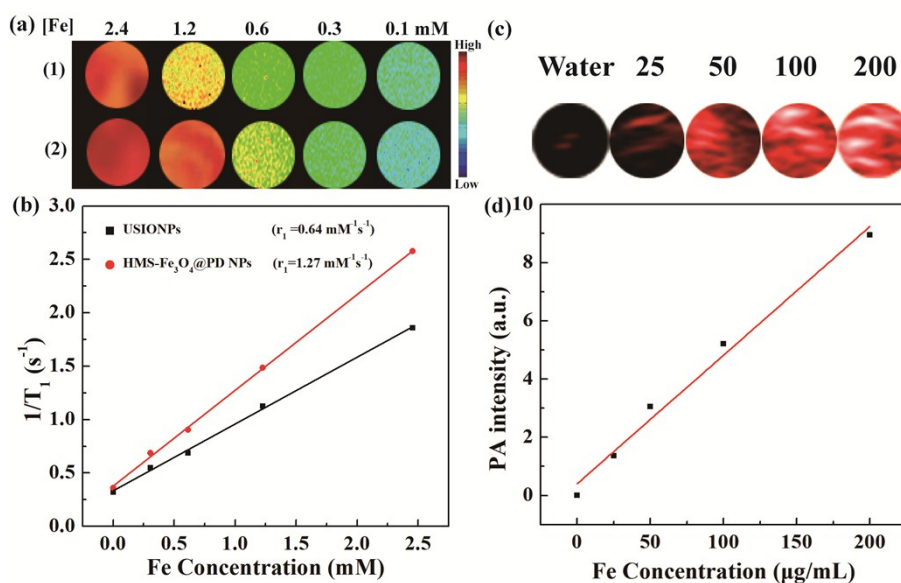


Fig. S3. (a) T₁-weighted MR images of Fe₃O₄ NPs and HMSs-Fe₃O₄@PD NPs at different Fe concentrations. Gradual increase in the MR signal intensity can be reflected from the color bar from blue to red. (b) Linear fitting of 1/T₁ versus Fe concentration of USIONPs and HMS-Fe₃O₄@PD NPs. (c) PA images and (d) PA values of HMS-Fe₃O₄@PD NPs at different Fe concentrations.

The signal intensity of T₁-weighted MR images was gradually enhanced with the increase of Fe concentration for both HMS-Fe₃O₄@PD NPs and USIONPs. The higher r₁ relaxivity of the HMS-

Fe₃O₄@PD NPs than that of the USIONPs might be because HMS NPs filled with USIONPs are able to increase the Fe concentration in a localized microenvironment, which is beneficial to increase their interaction with water. The surface PD coating does not seem to affect the accessibility of water protons to the surface of USIONPs due to the hydrophilic nature of the PD polymer.

The PA imaging performance of the HMS-Fe₃O₄@PD NPs reveals that with the increase of Fe concentration, HMS-Fe₃O₄@PD NPs afford the increased PA imaging signal intensity (Fig. S3c, ESI). The PA signal intensity of HMS-Fe₃O₄@PD NPs shows a linear relationship as a function of Fe concentration (Fig. S3d, ESI).

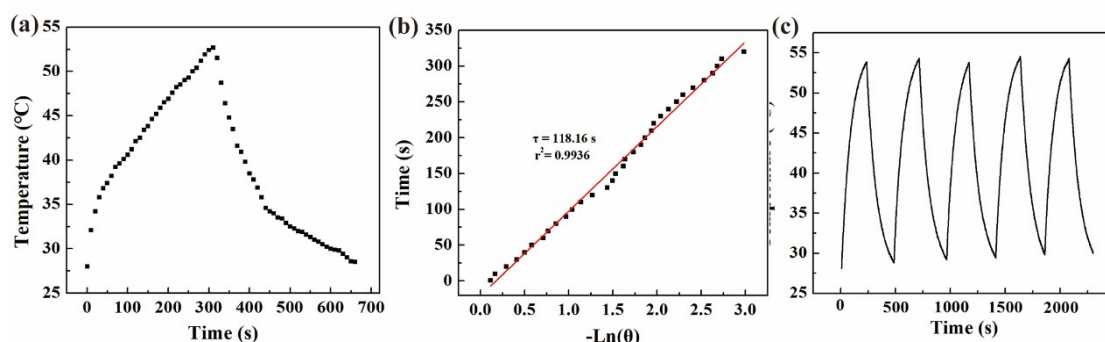


Fig. S4. (a) Photothermal effect of HMS-Fe₃O₄@PD NP aqueous solution irradiated by an 808 nm laser at a power density of 1.2 W/cm². The laser was turned off after irradiation for 300 s. (b) Plot of cooling time vs negative natural logarithm of the driving force temperature obtained from the cooling stage. (c) Real-time temperature elevation and cooling down of HMS-Fe₃O₄@PD solution in water (200 µg/mL, 100 µL) during 5 cycles of 808 nm NIR laser irradiation (1.2 W/cm²) for 260 s and cooling down for 190 s.

Photothermal conversion property measurements show that in contrast to water that does not show obvious temperature increase, the solution temperature of HMS-Fe₃O₄@PD NPs rapidly elevates under laser irradiation in a concentration-dependent manner (Fig. S4a, ESI). In particular, the temperature increases to 53.5 °C after 300 s of irradiation at the Fe concentration of 200 µg/mL, which is high enough to ablate cancer cells. In order to measure the photothermal conversion

efficiency (η) of HMS-Fe₃O₄@PD NPs, the aqueous solution of the NPs ([Fe] = 200 μ g/mL) was exposed to an 808 nm laser for 300 s and then the laser was turned off (Fig. S4a, ESI). In addition, the scale of temperature increase of the HMS-Fe₃O₄@PD NPs remained almost identical after at least five circles of heating and cooling down process (Fig. S4c, ESI), indicating their excellent photothermal stability.

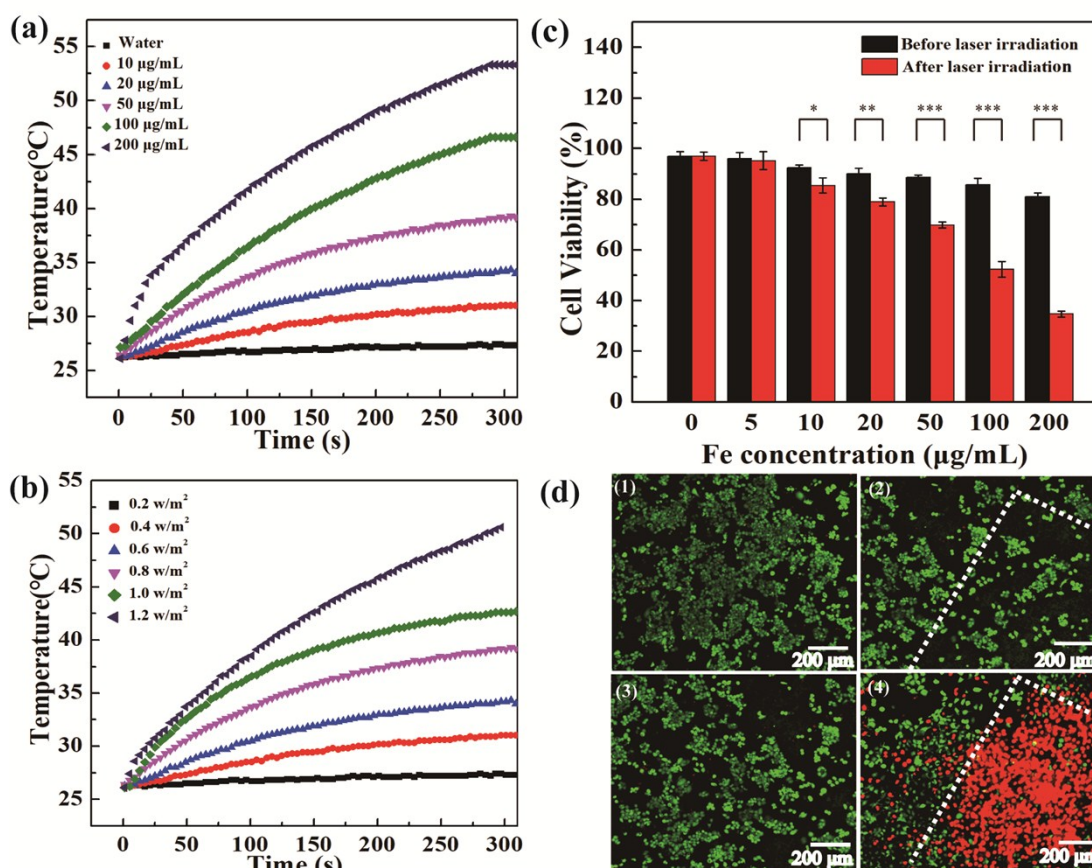


Fig. S5. (a) Temperature elevation curves of HMS-Fe₃O₄@PD NPs suspension at different Fe concentrations (Water, 10, 20, 50, 100 and 200 μ g/mL, respectively) under 808 nm laser irradiation at the power density of 1.2 W/cm² as the function of irradiation time. (b) Temperature elevation curves of HMS-Fe₃O₄@PD NPs suspension at the Fe concentration of 200 μ g/mL under 808 nm laser irradiation at different power densities (0.2, 0.4, 0.6, 0.8, 1.0 and 1.2 W/cm², respectively) as a function of irradiation time. (c) CCK-8 assay of 4T1 cell viability after treatment with the HMS-

Fe₃O₄@PD NPs at different Fe concentrations under 808 nm laser irradiation for 5 min. Data were represented as mean ± S.D. (n = 3). (d) Fluorescence microscopic images of Calcein AM/PI-stained 4T1 cells treated with PBS (1), PBS + 808 nm laser (2), HMS-Fe₃O₄@PD NPs at the Fe concentration of 200 µg/mL (3), and HMS-Fe₃O₄@PD NPs at the Fe concentration of 200 µg/mL + 808 nm laser (4). Scale bar in Panel (d) represents 200 µm. The margin of the laser facula region was distinguished by the white dotted line.

CCK-8 assay of 4T1 cell viability show that at the Fe concentration of 200 µg/mL, cells treated with the HMS-Fe₃O₄@PD NPs under laser irradiation (5 min) led to the decrease of cell viability to as low as 37.6%. Fluorescence microscopy data reveal that for the PBS-treated control cells with laser irradiation, nearly all the cells were healthy (green fluorescence). However, obvious cell death (red fluorescence) was observed after incubation with the HMS-Fe₃O₄@PD NPs under laser exposure. These data validated that the HMS-Fe₃O₄@PD NPs could be employed as a PTT agent for photothermal ablation of cancer cells in vitro.

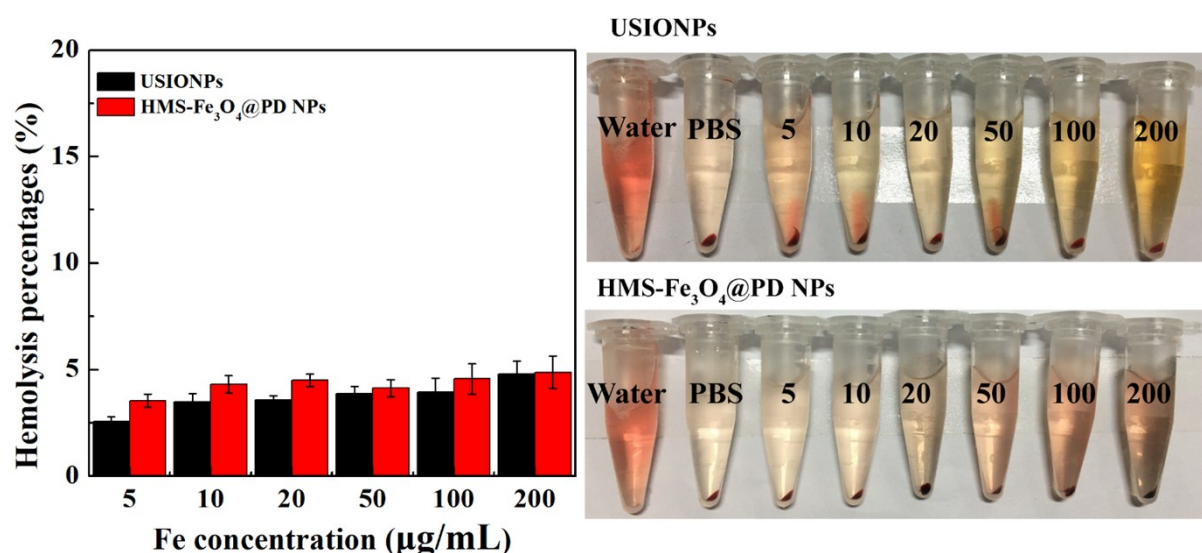


Fig. S6. Hemolysis percentages and photographs of the HRBC suspensions treated with USIONPs and HMS-Fe₃O₄@PD NPs at different Fe concentrations. The data are expressed as mean ± SD (n = 3). Water and PBS were used as positive and negative controls, respectively.

Hemolysis assay was performed to evaluate the hemocompatibility of USIONPs and HMS-Fe₃O₄@PD NPs. The results show that no significant hemolysis was observed for HRBCs after incubation with these NPs in the studied concentration range of 5-200 µg/mL. Quantitative analysis shows that the hemolysis rates of USIONPs and HMS-Fe₃O₄@PD NPs are all less than the threshold value of 5%, even at an Fe concentration as high as 200 µg/mL, indicating their excellent hemocompatibility.

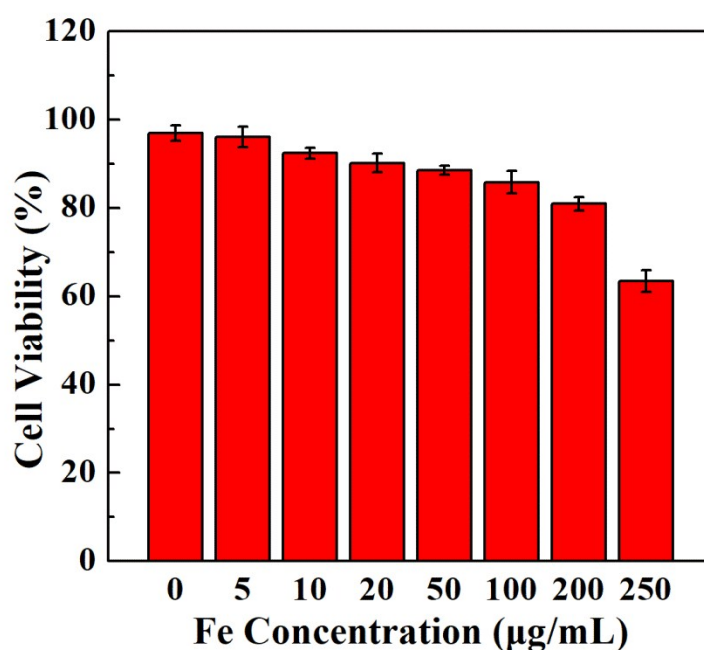


Fig. S7. CCK8 viability assay of 4T1 cancer cells treated with HMS-Fe₃O₄@PD NPs at different Fe concentrations. The cells treated with PBS were used as control. The data were expressed as mean ± SD (n = 3).

To confirm the cytocompatibility of the HMS-Fe₃O₄@PD NPs, CCK-8 assay was tested. We observe that the viability of 4T1 cells treated with the HMS-Fe₃O₄@PD NPs is above 80% at the Fe concentration ranging from 5 to 200 µg/mL. Only a slight cytotoxicity was seen when the Fe concentration was increased to 250 µg/mL.

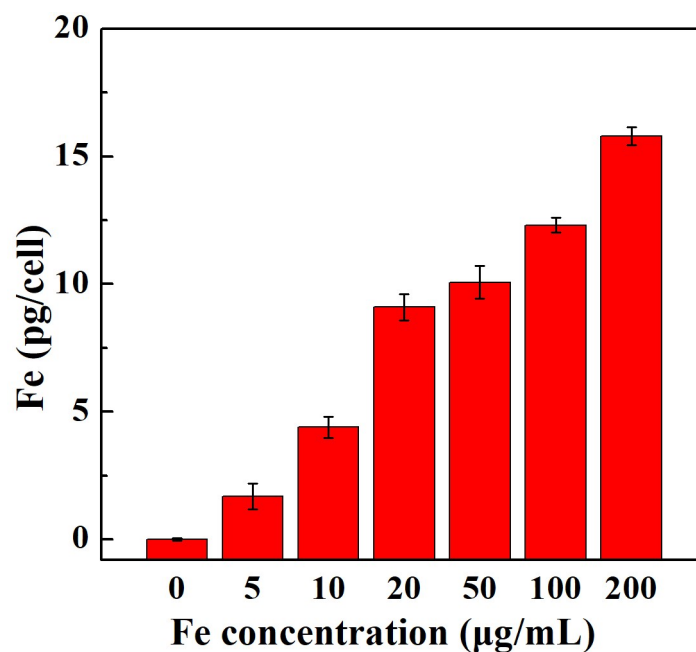


Fig. S8. Cellular uptake of Fe in 4T1 cells treated with the HMS-Fe₃O₄@PD NPs at different Fe concentrations for 12 h. Data are expressed as mean ± S. D. (n = 3).

To investigate the cellular uptake efficiency, 4T1 cells were incubated with the HMS-Fe₃O₄@PD NPs at different Fe concentrations for 12 h and the intracellular Fe content was measured using ICP-OES. As compared to the control cells, Fe content in the cancer cells after treatments with the HMS-Fe₃O₄@PD NPs increases in a concentration-dependent manner. At an Fe concentration of 200 µg/mL, the cellular Fe uptake reaches 15.79 pg/cell.

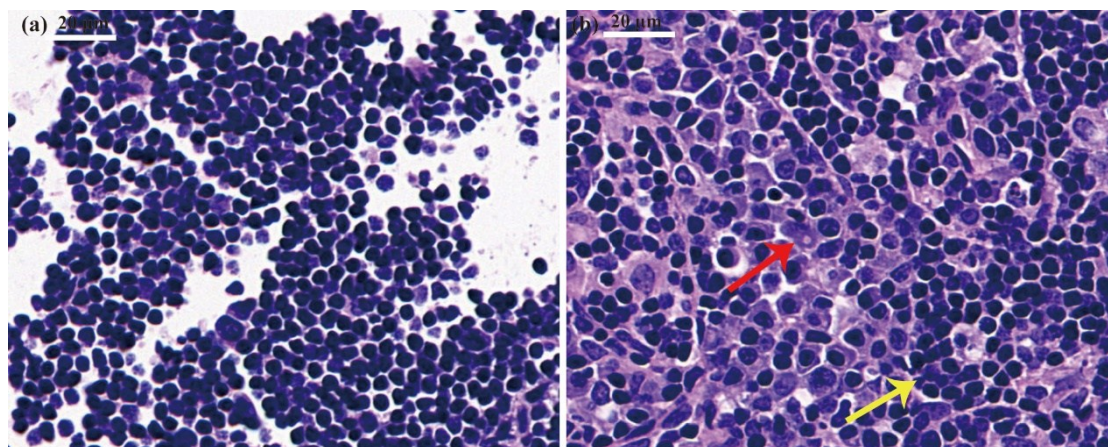


Fig. S9. H&E staining of normal lymph (a) and lymph infiltrated by tumor cells (b). Red is marked as tumor cells. Yellow is marked as normal lymph cells. The lymphatic tumor metastasis model was proven by H&E staining of normal lymphocytes and lymphocytes infiltrated by tumor cells.

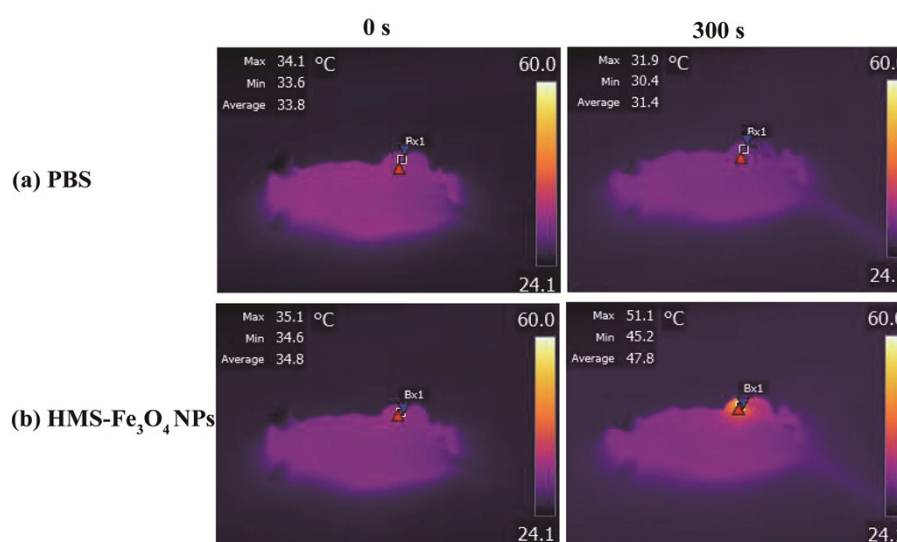


Fig. S10. Thermal imaging of tumor-bearing mice after intratumoral injection of (a) PBS (0.1 mL for each mouse) or (b) HMS-Fe₃O₄@PD NPs ([Fe] = 200 μg/mL, in 0.1 mL PBS for each mouse), followed by irradiation with an 808 nm laser (1.2 W/cm²) at time points of 0 and 300 s, respectively.

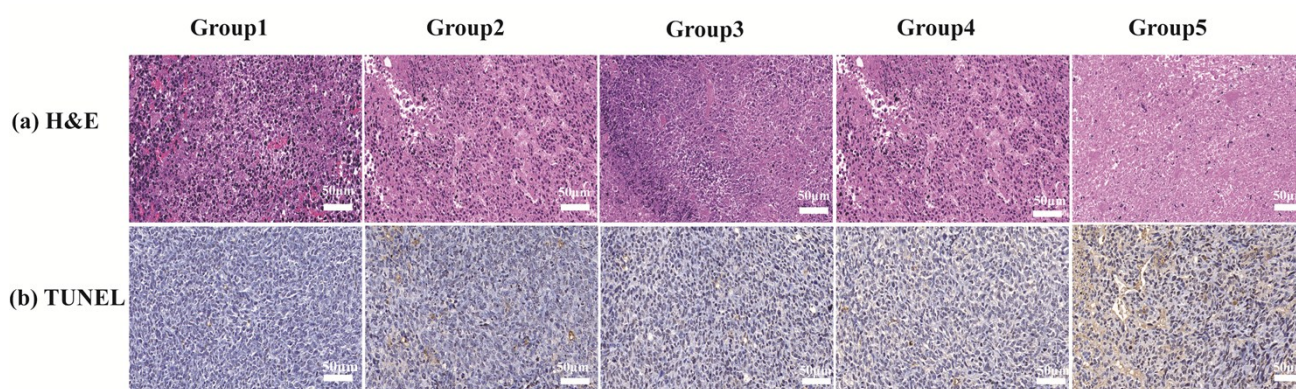


Fig. S11. H&E (a) and TUNEL (b) staining of tumor sections after different treatments. The scale bar shown in each panel represents 50 μm . The treatments are as follows: Group 1, control group (injection of with PBS); Group 2, injection of HMS-Fe₃O₄@PD NPs without PTT and RT; Group 3, RT; Group 4, injection of HMS-Fe₃O₄@PD NPs with PTT; Group 5, injection of HMS-Fe₃O₄@ PD NPs with PTT and RT.

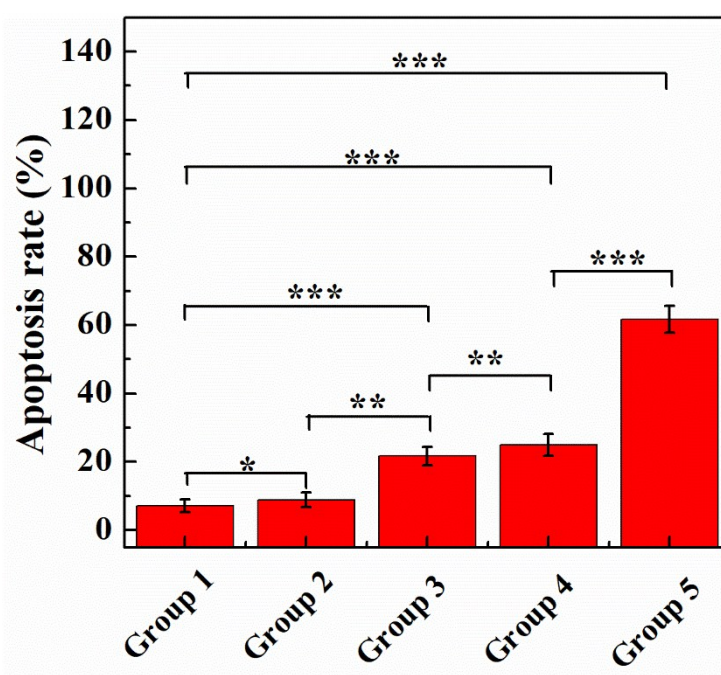


Fig. S12. Apoptosis rate of tumor cells after different treatments by quantification of the TUNEL-positive tumor cells in random tumor sections (data were represented as mean \pm S.D., n = 3). The treatments are as follows: Group 1, control group (injection of with PBS); Group 2, injection of HMS-Fe₃O₄@PD NPs without PTT and RT; Group 3, RT; Group 4, injection of HMS-Fe₃O₄@PD

NPs with PTT; Group 5, injection of HMS-Fe₃O₄@ PD NPs with PTT and RT. Quantitative analysis shows that the percentage of apoptotic cells in the Groups 1, 2, 3, 4 and 5 is 7.2%, 8.9%, 21.7%, 24.9% and 61.7%, respectively. Our results suggest that the PTT efficiency can be significantly enhanced after the combination with RT.

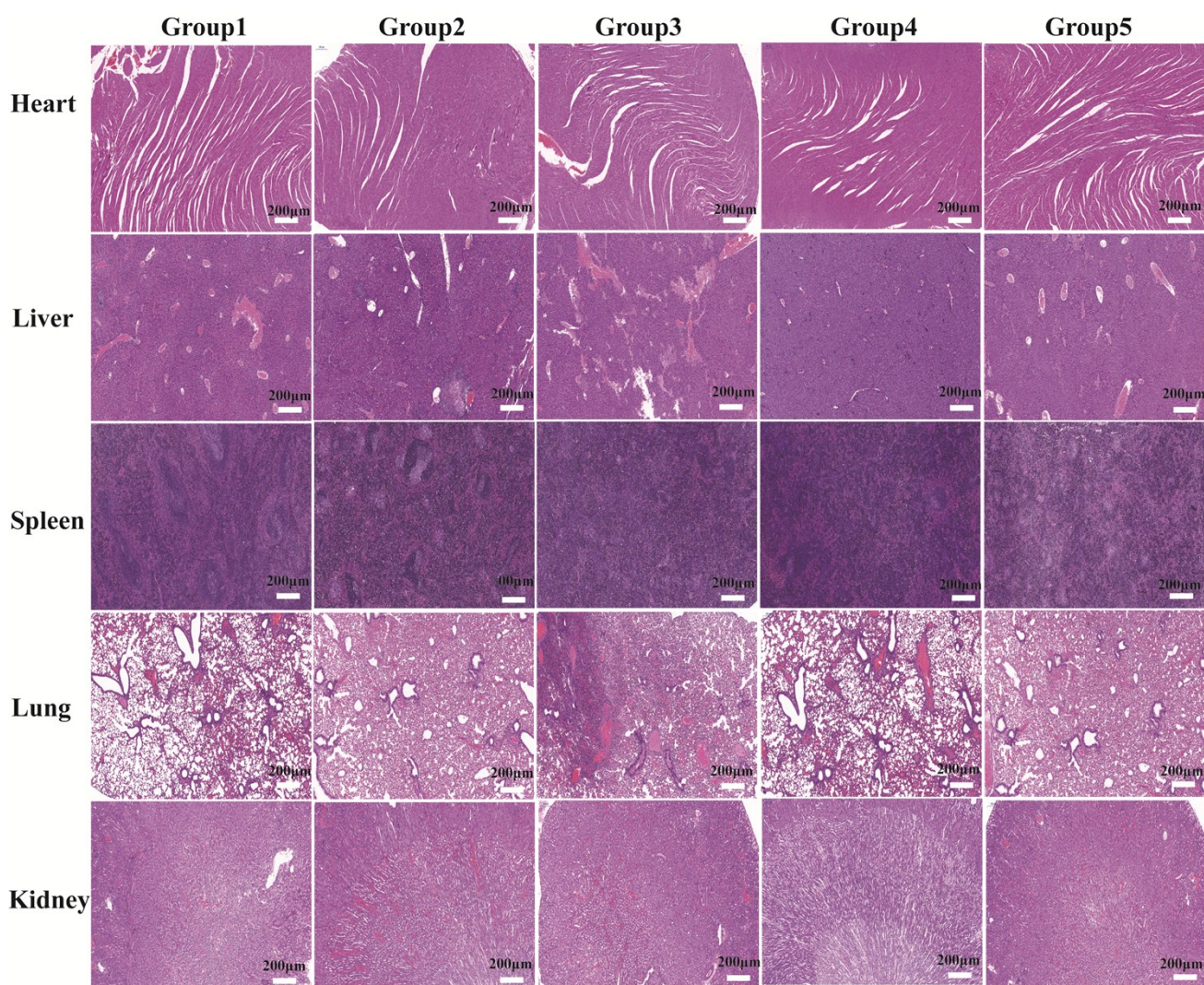


Fig. S13. H&E staining of major organs of mice. The treatments are as follows: Group 1, control group (injection of PBS); Group 2, injection of HMS-Fe₃O₄@PD NPs without laser irradiation and RT; Group 3, RT; Group 4, injection of HMS-Fe₃O₄@PD NPs with laser irradiation; Group 5, HMS-Fe₃O₄@PD NPs with laser irradiation and RT. The scale bar shown in each panel represents 200 μm.

Compared with the control group (Group 1), no abnormal change in the structures and morphologies of these organs in the mice after treatments was observed, indicating the negligible

adverse effects of PTT, RT, and combinational PTT/RT.

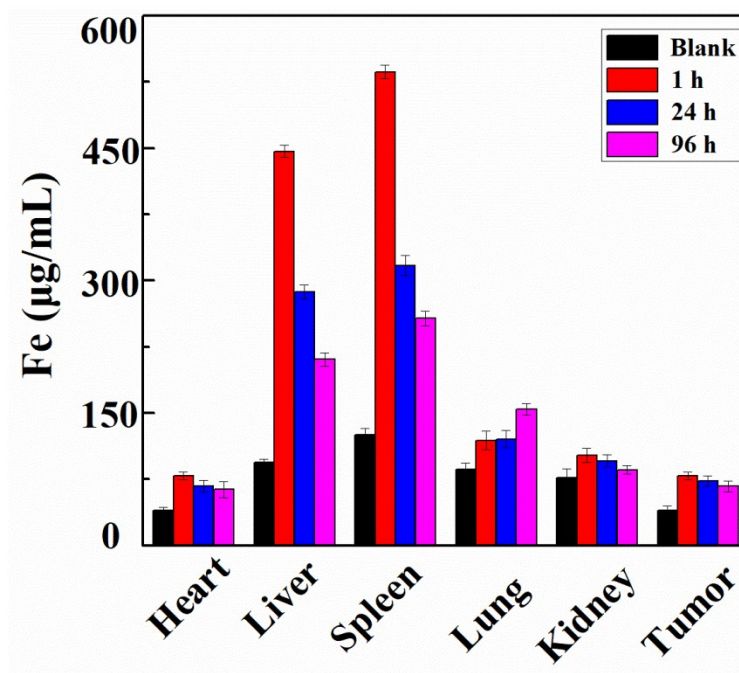


Fig. S14. Biodistribution of Fe element in tumor and the major organs of the mice including heart, liver, spleen, lung, and kidney (data were expressed as mean \pm S.D., $n = 3$). The data were recorded from the whole organ taken at different time points post intravenous injection of the HMS-Fe₃O₄@PD NPs ([Fe] = 200 $\mu\text{g}/\text{mL}$, 200 μL in PBS for each mouse).

We investigated the biodistribution of the injected NPs (Fig. S12, ESI). Liver (447.4 $\mu\text{g g}^{-1}$) and spleen (467.2 $\mu\text{g g}^{-1}$) were found to be well distributed with the HMS-Fe₃O₄@PD NPs at 1 h postinjection. Subsequently, Fe amount decreases in the major organs except lung at 24 h and 96 h postinjection, implying that HMS-Fe₃O₄@PD NPs could be metabolized and excreted with the time postinjection of the particles. These data suggest that the HMS-Fe₃O₄@PD NPs could be first cleared by the RES organs (e. g., liver and spleen), and a portion of the particles could escape from the RES organs and be taken up in the tumor tissue via passive EPR effect for effective tumor MR/PA imaging. Exact reason regarding the lung uptake of the particles is still unclear, which may deserve a long-term biodistribution study.

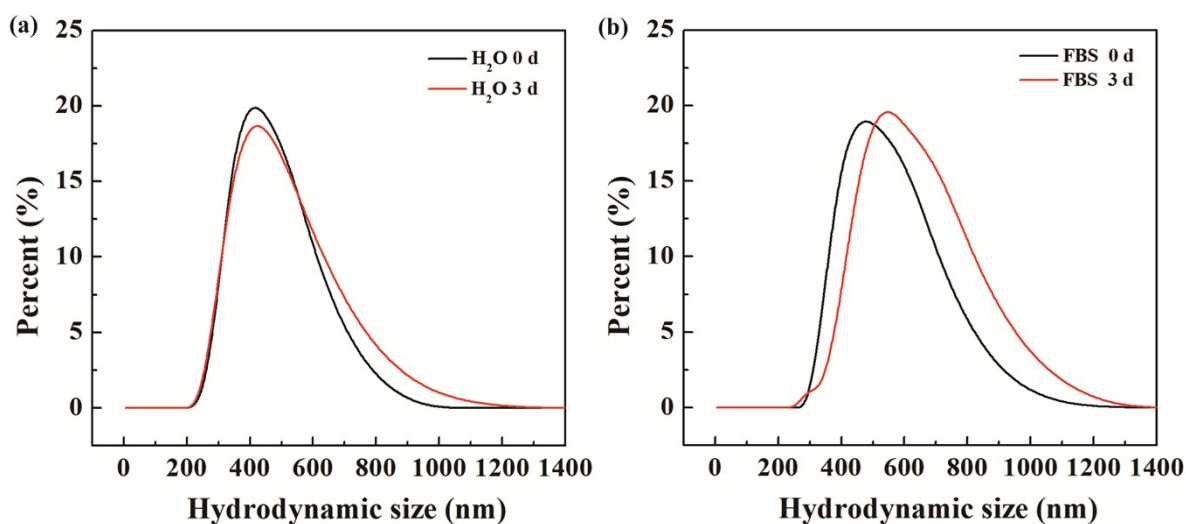


Fig. S15. Hydrodynamic size distribution of HMS-Fe₃O₄@PD NPs in water (a) and FBS (b) solution at 37 °C before and after 3 days.

References

1. D. Ma, J. W. Chen, Y. Luo, H. Wang and X. Y. Shi, *J. Mater. Chem. B*, 2017, **5**, 7267-7273.
2. Y. Chen, H. R. Chen, L. M. Guo, Q. J. He, F. Chen, J. Zhou, J. W. Feng and J. L. Shi, *Acs Nano*, 2010, **4**, 529-539.
3. H. Yang, Y. M. Zhuang, H. Hu, X. X. Du, C. X. Zhang, X. Y. Shi, H. X. Wu and S. P. Yang, *Adv. Funct. Mater.*, 2010, **20**, 1733-1741.
4. Y. Hu, R. Z. Wang, S. G. Wang, L. Ding, J. C. Li, Y. Luo, X. L. Wang, M. W. Shen and X. Y. Shi, *Sci. Rep.*, 2016, **6**, 28325.
5. C. Peng, L. F. Zheng, Q. Chen, M. W. Shen, R. Guo, H. Wang, X. Y. Cao, G. X. Zhang and X. Y. Shi, *Biomaterials*, 2012, **33**, 1107-1119.
6. Y. W. Zhou, Y. Hu, W. J. Sun, B. Q. Zhou, J. Z. Zhu, C. Peng, M. W. Shen and X. Y. Shi, *Nanoscale*, 2017, **9**, 12746-12754.
7. D. D. Shan, L. Chen, J. T. Njardarson, C. Gaul, X. J. Ma, S. J. Danishefsky and X. Y. Huang,

Proc. Natl. Acad. Sci. U. S. A., 2005, **102**, 3772-3776.

8. D. Li, Y. Zhang, S. Wen, Y. Song, Y. Tang, X. Y. Zhu, M. W. Shen, S. Mignani, J. P. Majoral, Q. Zhao and X. Y. Shi, *J. Mater. Chem. B*, 2016, **4**, 4216-4226.
9. J. C. Li, Y. Hu, J. Yang, P. Wei, W. J. Sun, M. W. Shen, G. X. Zhang and X. Y. Shi, *Biomaterials*, 2015, **38**, 10-21.